

Dry solid feeding characteristics by computational particle-fluid dynamics simulation at high pressure

Woo Chang Sung¹, Seok Woo Chung², SungKyu Lee³, Jong Sun Jung⁴,
Dong Hyun Lee^{5*}

^{1,5}School of Chemical Engineering, Sungkyunkwan University, Suwon, Republic of Korea

^{2,3}Institute for advanced engineering, Youngin, Republic of Korea

⁴Seintec Corporation, Hwaseong, Republic of Korea

Abstract— The parameters affecting particle injection in a high pressure powder fuel injection system were verified by using computational particle fluid dynamics (CPFD). The particles were coal ($\bar{d}_p=175 \mu\text{m}$, $\rho_s = 1350 \text{ kg/m}^3$), and the simulation was performed by changing the clearance between the roller and the hose and by changing the total pressure drop. Also, the wall erosion of the hose was confirmed by changing the clearance. As the clearance decreases from 10 mm to 1 mm when the total pressure difference is 10 bar, it is confirmed that the injection of the particles is increased two-fold, but the power of the motor should be increased to 1.45 times. When the clearance is 5mm, as the total pressure drop is increased from 10 bar to 30 bar, the particle injection rate decreases 0.33-fold, but the motor power must be increased 3-fold. Also, it was confirmed that the wall erosion of the hose was large when the clearance was 7 mm or more.

Keywords— Dry solid feeding, high pressure, simulation, Clearance, Backflow.

I. INTRODUCTION

Many devices in the chemical process operate at high pressure rather than atmospheric pressure. In the case of the gas phase reaction, a high pressure induces large gas density. Therefore, a greater amount of gas can be added, which leads to an increase in the production amount. Recently, the Integrated Gasification Combined Cycle (IGCC), which has been attracting attention due to its low carbon policy, has shown high efficiency as well as low SO_x, NO_x, and CO₂ emissions compared to coal-fired power generation. However, the disadvantage of IGCC is its high cost compared to existing coal-fired power plants. Coal injection contributes about 43%-45% of the high cost of IGCC [1]. In the IGCC, it is necessary to inject coal from atmospheric pressure to high pressure; however, a general injection device cannot inject particles from atmospheric pressure to high pressure. This is due to the difficulty of injecting particles from atmospheric pressure to high pressure because the gas flows from a high pressure to a low pressure. In order to solve the problem of the backflow of gas, a lock hopper method is generally used when injecting particles from atmospheric pressure to high pressure. The advantage of the lock hopper method is that it can overcome a large pressure difference and can transfer the particles. However, the lock hopper method has disadvantages, since it is difficult to continuously inject particles because the pressurization and decompression must be repeatedly performed. Also, the lock hopper method requires equipment that is considerably large and relatively expensive in terms of construction and operating costs [2-5]. For example, in Shell's IGCC plant in Buggenum, which the existing lock hopper method is used, the cost of the coal injection part is estimated to be about 0.1 billion dollar [1]. Accordingly, a high-pressure powder fuel injection device has been developed to replace the lock hopper method injection device [1]. Stamet and Rocketdyne are developing the posimetric pump and the dry solid pump, respectively [1].

In this study, the experiment was carried out for the case of an atmospheric pressure condition, and the total pressure drop is 10 bar. However, it is difficult to find the variables that may affect the higher pressures and injection rate. In addition, to check the wall erosion of the hose, the hose must be operated for a long time; therefore, the wall erosion needs to be predicted for validity analysis. Therefore, in this study, we predicted the solid transfer characteristics of a high-pressure powder injector by using computational particle fluid dynamics (CPFD) method using the multi-phase particle-in-cell (MP-PIC) method.

II. EXPERIMENT AND SIMULATION

2.1 Experimental

Experiments were conducted using coal for verification of the simulation data. The specifications of the experimental apparatus are shown in **Figure 1**. A compression roller is installed in the chain, and the rotational force of the electric motor

is transmitted to the chain to rotate the compression roller. The upper hopper is filled with coal and the lower roller is compressed. At the same time, the high-pressure hose is pressed to transfer the coal in the high pressure hose to the lower hopper by the pushing force of the compression roller. The clearance between the hose and the roller was 10 mm. The speed of the roller was changed to 0 - 0.12 m / s using a motor inverter and the pressure of the lower hopper was changed to 10 bar at atmospheric pressure.

The injected rate was calculated using the mass value of the sample measured, using a load cell for 10 minutes under each condition.

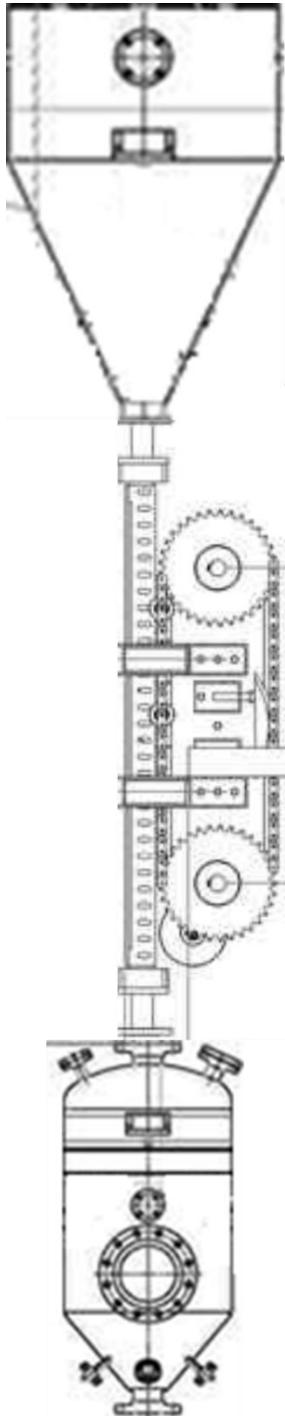


FIGURE 1. SCHEMATIC DIAGRAM OF EXPERIMENT



FIGURE 2. 3D DIMENSION OF HOSES THAT ARE PUSHED BY ROLLER. (A): REALIZATION MODEL, (B): SIMPLIFICATION MODEL

2.2 Governing equation

The CPF method calculates the momentum of particles and fluids in three dimensions. The fluid is calculated using the Navier-Stokes equation and the particle is calculated using the MP-PIC numerical method. The phases of the fluid and the solid are considered together by calculating the drag force between the phases. The phase of the fluid is solved by the governing equations.

$$\frac{\partial}{\partial t}(\rho_f \theta_f) + \nabla \cdot (\rho_f \theta_f v_f) = S_f \quad (1)$$

For incompressible fluids, the momentum equation is expressed as (2).

$$\frac{\partial}{\partial t}(\rho_f \theta_f u_f) + \nabla \cdot (\rho_f \theta_f v_f v_f) = -\nabla p - F + \rho_f \theta_f g + \nabla \theta_f \tau_f \quad (2)$$

where ρ_f is the fluid density, θ_f is the volume fraction, v_f is the fluid velocity, and S_f is related to the fluid mass. τ_f is the fluid stress tensor, g is the gravity acceleration, and F is the ratio of momentum exchange in solid and fluid. F is calculated using equation (3).

$$F = \iiint f V_p \rho_p \left[D_p (v_f - v_p) - \frac{1}{\rho} \nabla p \right] dV_p d\rho_p dv_p \quad (3)$$

where v_p is the particle velocity, ρ_p is the particle density, D_p is the drag function depending on the particle position, and f is a probability density function calculated using the Liouville equation. The particle acceleration is calculated using the Lagrangian method.

$$\frac{dv_p}{dt} = D_p (v_f - v_p) - \frac{1}{\rho_p} \nabla P + g - \frac{1}{\theta_p \rho_p} \nabla \tau_p \quad (4)$$

In equation (4), the value of D_p is calculated using the drag model. The Wen-Yu Ergun model of Gidaspow is used, which combines the Wen and Yu model, known to be well suited for the dilute system. Also, the Ergun model is used, which is known to fit well in the packing system. Equation (5) represents the expression of the drag model.

$$D = \begin{cases} D_1, & \theta_p < 0.75\theta_{CP} \\ (D_2 - D_1) \left(\frac{\theta_p - 0.75\theta_{CP}}{0.85\theta_{CP} - 0.75\theta_{CP}} \right) + D_1, & 0.75\theta_{CP} \leq \theta_p \leq 0.85\theta_{CP} \\ D_2, & \theta_p > 0.85\theta_{CP} \end{cases} \quad (5)$$

where θ_p is the particle volume fraction and θ_{cp} is the volume fraction when the particles are packed at maximum. D_1 is calculated using the Wen and Yu drag model.

$$D_1 = \frac{3}{8} C_d \frac{\rho_f |u_f - u_p|}{\rho_p r_p} \quad (6)$$

where C_d is the drag coefficient and is calculated using equation (7).

$$C_d = \begin{cases} \frac{24}{Re} \theta_f^{-2.65} & Re < 0.5 \\ \frac{24}{Re} \theta_f^{-2.65} (1 + 0.15 Re^{0.687}) & 0.5 \leq Re \leq 1000 \\ 0.44 \theta_f^{-2.65} & Re > 1000 \end{cases} \quad (7)$$

The Ergun equation is expressed as equation (8).

$$D_2 = 0.5 \left(\frac{C_1 \theta_p}{\theta_f Re} + C_2 \right) \frac{\rho_f |u_f - u_p|}{\rho_p r_p} \quad (8)$$

2.3 Modeling of apparatus

A schematic diagram of the 3D dimension for simulating the experimental setup used in this study with CPF is shown in **Figure 2**. The diameter of the hose is 0.04 m, the height is 1.45 m, and the thickness is 0.0125 m. The diameter of the roller pressing the hose is 0.16 m, and the distances between the first roller and the next roller are arranged at 0.3 m intervals. Based on the above information, a realization model is used when the roller presses the hose, and a simplification model is used that simplifies the cylindrical hose to a rectangular parallelepiped. In the case of the simplification model, the horizontal and vertical lengths of the rectangular parallelepiped are adjusted. As a result, the parallelepiped was simplified to a hose with a width of 0.035 m, a length of 0.035 m, and a height of 1.45 m.

2.4 Simulation condition

The average particle size of the particles used in the simulation was $175\ \mu\text{m}$, the density was $1350\ \text{kg/m}^3$, and air was used as the gas. The volume fraction of the particles was set at 0.6. The variables considered to be significant in the simulation are the clearance and total pressure difference between the inlet and outlet. The clearance was changed to 1-10 mm and the pressure drop was changed to 10-30 bar.

III. RESULTS AND DISCUSSION

3.1 Experiment result

When the clearance between the hose and the roller is 10 mm using coal, the injection rate according to the roller speed is confirmed when the total pressure difference is 0 bar and 10 bar. As shown in **Figure 3**, the injection rate increases linearly with the roller speed at each pressure condition. However, it was confirmed that the injection rate decreased more when the total pressure drop was 10 bar than when the pressure drop was 0 bar. This is considered to be because, as the pressure at the lower end increases, the gas at the lower end is forced to flow backward due to the pressure difference, and the particles must descend to overcome the force.

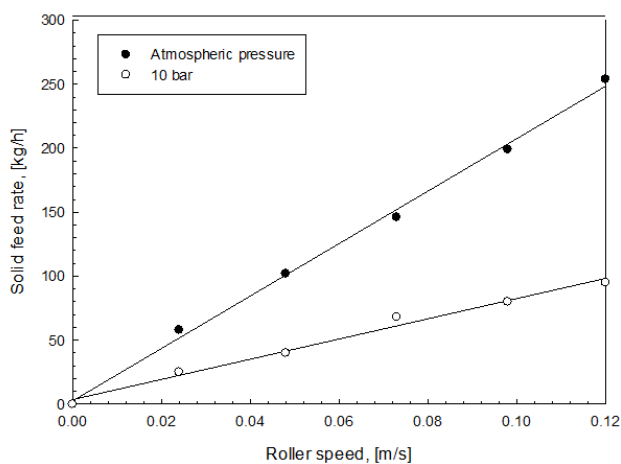


FIGURE 3. ROLLER SPEED VERSUS SOLID FEED RATE

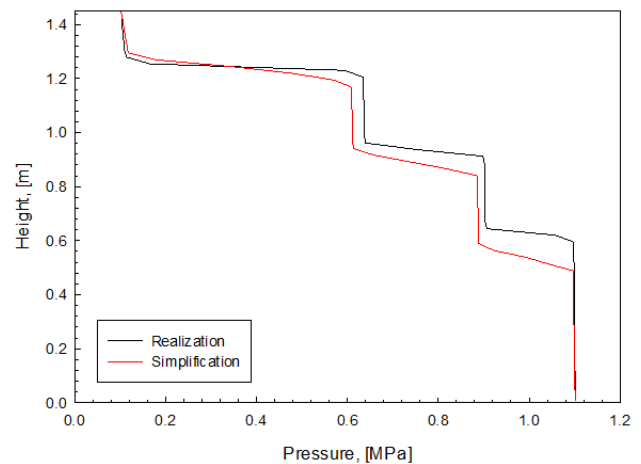


FIGURE 4. PRESSURE PROFILE OF REALIZATION AND SIMPLIFICATION

3.2 Comparison of realization and simplified model

In order to verify the validity of the simplified model, a simulation of the realization model is shown in **Figure 4**. By comparing the pressure drops among the rollers, an error of about 7% was found in the first roller at the bottom, 3% in the second roller, and 13% in the third roller. Although the contact areas of the rollers are the same, because the cylindrical roller is simplified into a rectangular parallelepiped, the difference is caused by the difference in height among the rollers. In addition, unlike the simplified model, the rubber hose is not pressed radially; rather, the pressure drop among the rollers differs from the actual model because the roller hose is gradually depressed according to the height of the roller. Likewise, the rubber hose is simplified to a rectangular parallelepiped in a simplified model, but the actual model is a cylinder. In the simplified model, the area pressed by the roller is constant, but in the actual model, the section which becomes extremely thin is generated. Therefore, in the simplified model, the pressure drop applied to the pressed part is constant according to the height, but in the actual model, the pressure drop according to the height increases in the narrower part. Increasing the pressure drop at the narrower part means that the force applied to the narrower part increases and eventually the entire the roller is not subjected to the same force but the part where the hose is pressed deeply under goes a larger force. However, the main purpose of this study is not to confirm the absolute value of the pressure drop, but to observe the change of the pressure drop according to the clearance or the tendency to change according to the total pressure. In addition, because the difference among the values is within 13% maximum, it can be confirmed that the simplified model can explain relation pressure drop and clearance. Consequently, the simulations were carried out using a simplified model.

3.3 Pressure profile according to clearance

Figure 5 shows the simulation results according to clearance and total pressure drop. Clearance refers to the distance between the roller and the hose at the roller contact distance. As can be seen in the graph, as the clearance is decreased, the

difference in pressure between the lower part and the upper part of the roller increases. On the other hand, the difference in pressure at the portion where the roller is not pressed decreased as the clearance decreased. When the clearance was 1mm, the pressure drop from the lower end of the hose to the lower end of the first roller at the lower end was 4.8 kPa and the pressure drop at the first lower roller was 207.7 kPa. When the clearance was 10 mm, the pressure drop from the lower end hose to the lower part of the first roller at the lower end was 71.4 kPa and the pressure drop at the first lower roller was 150.9 kPa. As the pressure drop at the portion where the roller is not pressed is increased, the possibility that the high-pressure gas at the lower end flows backward increases. As the width of the clearance is reduced, the stable particle injection becomes more advantageous, but as the width of the clearance is reduced, the pressure drop on the roller increases. The pushing force of the roller is proportional to the pressure drop applied to the roller, which is 1.38 times greater than 1 mm when the clearance is 10 mm. In other words, when the clearance is 10 mm, the force applied to the roller is greater as the pressure drop is larger at 10 mm than the 1 mm clearance; therefore, a greater force is required to drive the roller. By comparing the pressure drops applied to roller when clearance is 1 mm, it was confirmed that a high pressure drop was applied when position of roller goes up, 207.7 KPa in the lower part, 272.7 KPa in the middle part, and 490.9 KPa in the upper part. That is, the upper roller receives more force because of the relationship between the volume and the pressure of the gas. The volume of the gas increases as the pressure decreases, and the velocity of the gas increases due to the increased volume. As the velocity of the gas increases, the energy of the gas increases and it is confirmed that the upper roller undergoes a greater pressure drop. Comparing the pressure drop of the roller due to the pressure drop between the upper and lower parts, the sum of the pressure drop across the three rollers is 9.7 bar when the total pressure drop is 10 bar and clearance is 1 mm, and is 29.3 bar when the total pressure drop is 30 bar and the clearance is 1 mm. The roller pressure was 3.02 times. For a total pressure drop of 10 bar and a clearance of 10 mm, a pressure differential of 3.08 times greater was loaded to the roller. As the clearance increases, the pressure drop increase of the roller decreases as the total pressure increases. On the other hand, when the clearance is 1 mm, the pressure drop increases 2.43 times, while it increases 2.83 times at 10 mm. As the total pressure drop increases, the possibility of backflow of the gas increases, but if the clearance is narrow, the rate of increase of the pressure drop at the portion where the roller is not pressed is reduced. Therefore, when the clearance is narrow, it is relatively easy to inject particles at high pressure.

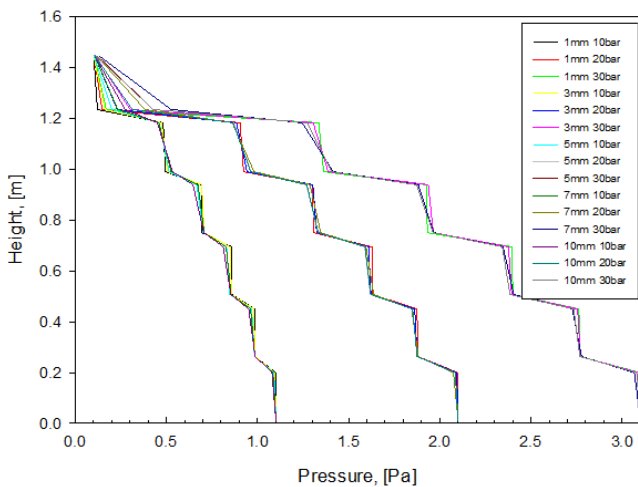


FIGURE 5. PRESSURE PROFILE WITH VARIED CLEARANCE AND TOTAL PRESSURE DROP

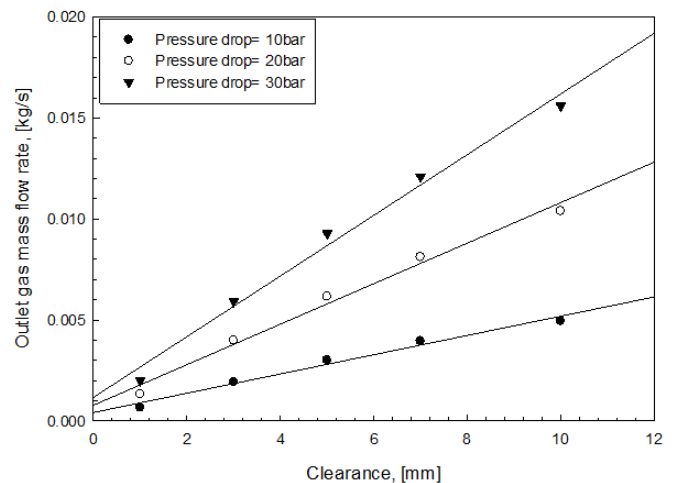


FIGURE 6. REVERSE GAS FLOW RATE WITH CHANGING CLEARANCE AND TOTAL PRESSURE

3.4 Backflow of gas

Figure 6 shows the amount of backflow of gas at the top of the high-pressure powder fuel injector according to the clearance and total pressure.

The gas backflow rate increased with increasing clearance and total pressure drop. The data of the gas backflow amount is plotted with the differential pressure data from the hose where the roller is not pressed.

$$\text{Outlet gas mass flow rate} \left[\frac{\text{kg}}{\text{s}} \right] = 0.0166 \left[\frac{\text{kg}}{\text{s} \cdot \text{MPa}} \right] * \text{Pressure drop}(\text{MPa}) - 0.001 \tag{9}$$

That is, it can be seen that as the pressure drop of the portion of the hose where the roller is not pressed increases, the gas backflow increases. The differential pressure of the hose part where the roller is not pressed can be calculated by equation (9).

$$\text{Pressure drop}[MPa] = \text{Total pressure}[MPa] * (0.0322 * \text{Clearance}[mm] - 0.0188) + 0.1224 \quad (10)$$

It can be seen that the pressure drop increases when the clearance increases or when the total pressure drop increases. As the back flow of the gas increases, the mass flux of the downward flow of the solid particles must be increased in order to prevent the back flow of the gas under the actual operating conditions. Determining the solid mass flux is related to the speed of the roller. As the speed of the roller increases, the amount of dragging and dropping of particles during the same time increases, and the solid mass flux value increases; this can prevent gas backflow.

3.5 Wall erosion of hose

The above sections describe the power and speed of the motor according to clearance and the total pressure. This section discusses the wall erosion of the hose. If a problem arises when the erosion of the hose becomes serious, shutdown then must be frequently performed while operating the process, which results in increasing costs. Therefore, it is very important to know the conditions that cause the erosion. Equation (11) is used to calculate the wall erosion and is based on the default value provided by CPFDF.

$$\text{Wall erosion} = f(\theta) * m_s^{1.5} * v_p^{3.5} \quad (11)$$

Where m is the mass of the particle, v is the velocity of the particle, and $f(\theta)$ is the value dependent on the angle. The wall erosion value is a relative value used to analyze the location of the wall erosion and the conditions under which further wall erosion would occur. **Figure 7** shows the wall erosion profile versus height, changing the clearance. In all cases, the wall erosion of the hose occurred at the part where the roller was pressed. At the point where the roller begins to be pressed, the velocity of the gas increases, and the velocity of the particle increases, causing considerable wall erosion. Also, at the end of the roller, the accelerated particles dispersed and caused erosion on the hose. On the other hand, the wall erosion value was very large when the clearance was 7 mm or more. As can be seen in **Figure 8**, when the clearance is greater than 7 mm, the movement of the particles in the x-direction is freer and the particle x velocity value is increased compared to when the clearance is narrow. The increase in particle x velocity resulted in more erosion effects than with particle z velocity; this caused a greater amount of erosion with a clearance greater than 7 mm.

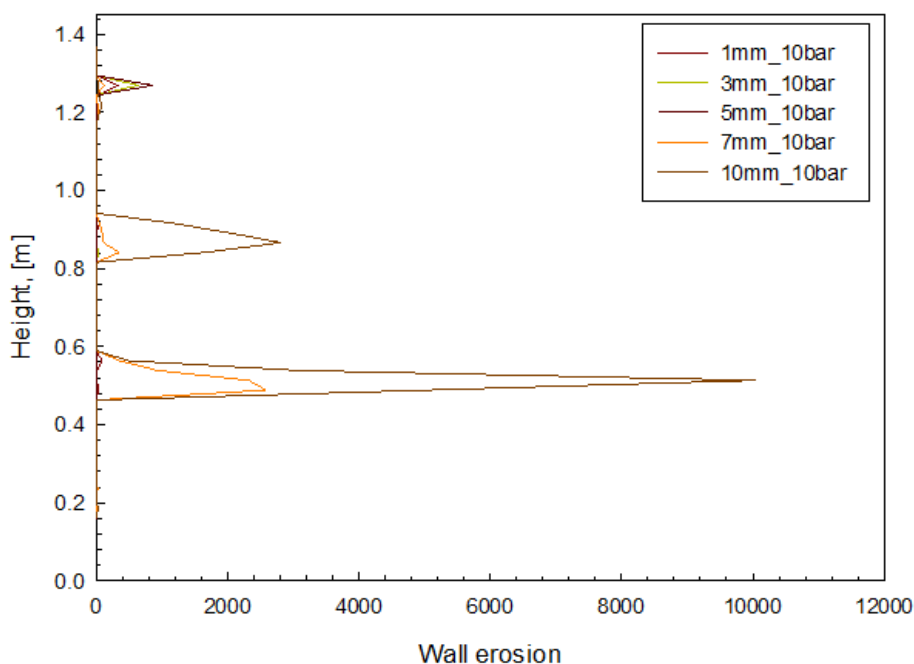


FIGURE 7. WALL EROSION VERSUS AXIAL HEIGHT WITH CHANGING CLEARANCE

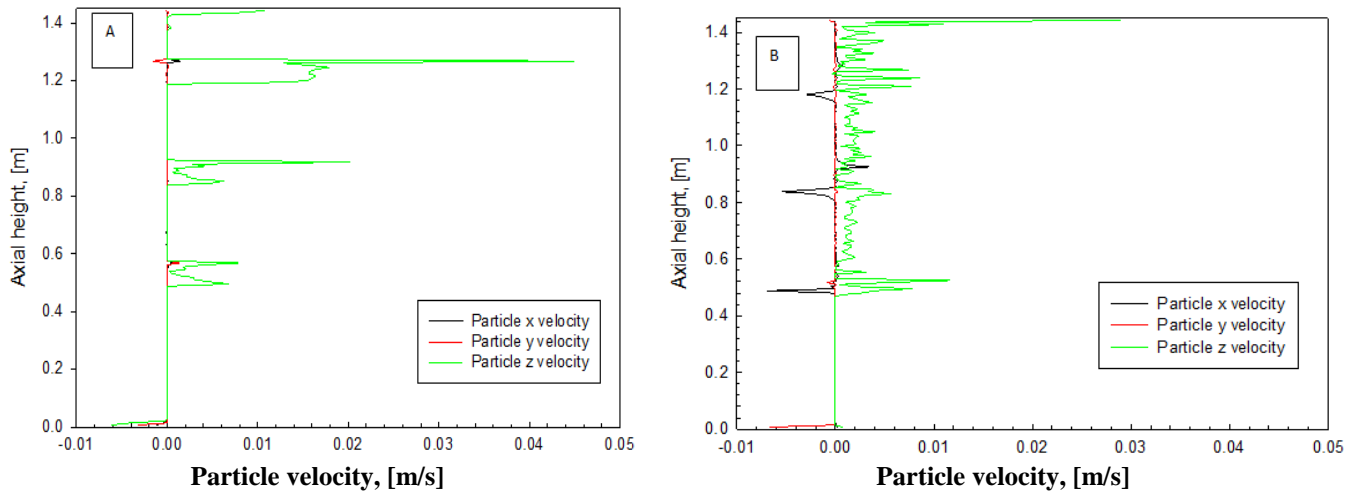


FIGURE 8. PARTICLE VELOCITY VERSUS AXIAL HEIGHT

3.6 Prediction of high pressure powder fuel injection system using CFPD

Simulation shows the effect of clearance and total pressure difference. In the experiment mentioned in Section 3-1, the injection amount (\dot{m}_s) of the particles according to the speed (0.024-0.12 m/s) of the roller at the atmospheric pressure is expressed by equation (13) at equation (12) and 10 bar.

$$\text{Solid mass flow rate}(\dot{m}_s) \left[\frac{\text{kg}}{\text{s}} \right] = 2049.3 \left[\frac{\text{kg}}{\text{m}} \right] \times \text{Roller speed} \left[\frac{\text{m}}{\text{s}} \right] + 2.5168 \quad (12)$$

$$\text{Solid mass flow rate}(\dot{m}_{s,10\text{bar}}) \left[\frac{\text{kg}}{\text{s}} \right] = 789.15 \left[\frac{\text{kg}}{\text{m}} \right] \times \text{Roller speed} \left[\frac{\text{m}}{\text{s}} \right] + 3.5896 \quad (13)$$

The slopes of equation (13), i.e., the weights of the particles per unit length, were compared using data obtained from CFPD to experiment. Assuming that the gas backflow is zero at normal pressure, the weight of particles per unit length is 2049.3 kg/m and the weight of particles per unit weight is 789.15 kg/m when the backflow is 0.4256 kg/s. Based on this data, **Table 1** shows the predicted motor force based on the predicted value of clearance and the particle weight per unit weight for the total pressure drop and the pressure drop on the roller, with 10 bar and clearance 10 mm as references. If the roller is operated at 20 bar at intervals of 10 mm, then it is not operating normally because it has a value of -0.108.6 kg/m. It can be seen that it is possible to reduce the gap to 5 mm or less in order to obtain a similar injection amount. However, the decrease in clearance increases the pressure drop of the roller, which means that the power of the motor increases. For example, if the clearance is 5 mm at 20 bar, the motor power needs to increase 2.53 times more than the reference.

TABLE 1
PREDICTED VALUE OF MASS PER UNIT LENGTH AND POWER RATIO

Pressure, [MPa]	Clearance, [mm]	Mass per unit length, [kg/m]	power ratio, [-]
0	10	2049.3	
1	10	789.1	1.00
1	7	1075.2	1.14
1	5	1265.8	1.25
1	3	1456.5	1.35
1	1	1647.2	1.45
2	10	-108.6	2.05
2	7	463.4	2.32
2	5	844.8	2.53
2	3	1226.2	2.72
2	1	1607.5	2.91
3	10	-1006.3	3.08
3	7	-148.3	3.53
3	5	423.8	3.82
3	3	995.8	4.10
3	1	1567.9	4.37

IV. CONCLUSION

CPFD simulations were carried out to identify the variables affecting the operation of the high-pressure powder fuel injection system and to understand the effect of the variables. It was found that as the clearance increased, the backflow of the gas also increased. However, as the clearance increased, the pressure drop on the roller decreased, so the load on the motor was reduced. On the other hand, CPFD simulation predicted that a clearance of 5mm or less should be maintained for the wall erosion of the hose, since a clearance of 7mm or more is expected to cause significant erosion.

ACKNOWLEDGMENT

This work was supported by a grant from the Korea Institute of Energy Technology Evaluation and Planning (KETEP), funded by the Ministry of Trade, Industry and Energy (MTIE) of the Korea government (No. 20163010050070).

NOMENCLATURE

\bar{d}_p	Sauter mean diameter [\square m]	m_s	Mass of solid [kg]
ρ_s	Solid density [kg/m^3]	θ	Angle of collision [$^\circ$]
ρ_p	Particle density [kg/m^3]	S_f	Interpolation operator [-]
ρ_f	Fluid density [kg/m^3]	τ_f	Stress tensor of fluid [Pa]
θ_p	Particle volume fraction [-]	g	Gravitational acceleration [m/s^2]
θ_{cp}	Close pack particle volume fraction [-]	F	Momentum exchange rate per volume between the fluid and solid phases [$\text{Pa}^*\text{s}/\text{m}$]
θ_f	Fluid volume fraction [-]	D_p	Interphase drag coefficient [m/s^2]
v_f	Fluid velocity [m/s]	f	Particle distribution function [-]
v_p	Particle velocity [m/s]	C_d	Drag coefficient [-]
\dot{m}_s	Solid mass flow rate [kg/s]		

REFERENCES

- [1] Amin, S. M., & Wollenberg, B. F. (2005). Toward a smart grid: power delivery for the 21st century. *IEEE power and energy magazine*, 3(5), 34-41.
- [2] Anthony, E. J. (1995). Fluidized bed combustion of alternative solid fuels; status, successes and problems of the technology. *Progress in Energy and Combustion Science*, 21(3), 239-268.
- [3] Li, X. T., Grace, J. R., Lim, C. J., Watkinson, A. P., Chen, H. P., & Kim, J. R. (2004). Biomass gasification in a circulating fluidized bed. *Biomass and bioenergy*, 26(2), 171-193.
- [4] Marcus, R. D. (2012). *Pneumatic conveying of solids*. Springer Science & Business Media.
- [5] Dai, J., Cui, H., & Grace, J. R. (2012). Biomass feeding for thermochemical reactors. *Progress in Energy and Combustion Science*, 38(5), 716-736.
- [6] Wen, CY (1966) Mechanics of fluidization. In *Chem. Eng. Prog. Symp. Ser.* (Vol. 62, pp. 100-111).
- [7] Ergun, S. (1952). Fluid flow through packed columns. *Chem. Eng. Prog.*, 48, 89-94.
- [8] Gidaspow, D. (1994). *Multiphase flow and fluidization: continuum and kinetic theory descriptions*. Academic press